LAND SUBSIDENCE IN WUHAN REVEALED USING A MULTI-SENSOR INSAR TIME SERIES FUSION APPROACH

Haonan Jiang[a,b], Timo Balz[a], Jianan Li[c]

a State Key Laboratory of Information Engineering in Surveying, Mapping and Remote Sensing (LIESMARS), Wuhan University, 430079 Wuhan, China
b Helmholtz Centre Potsdam, GFZ German Research Centre for Geosciences, 14473 Potsdam, Germany
c School of Geomatics, Liaoning Technical University, Fuxin 123000, China

KEY WORDS: InSAR, Power exponential knothe model, Long short-term memory network, Data fusion, Urban subsidence.

ABSTRACT:

Satellite Interferometric Synthetic Aperture Radar (InSAR) is widely utilized for topographic, geological, and natural resource investigations. However, many existing InSAR studies on ground deformation are limited to relatively short observation periods and single sensors. This paper introduces a novel method for fusing multi-sensor InSAR time series data, specifically designed to address scenarios involving partial overlaps and temporal gaps. The method employs a new Power Exponential Knothe Model (PEKM) to fit and fuse overlaps in the deformation curves, while a Long Short-Term Memory (LSTM) neural network predicts and fuses data during temporal gaps in the series. In this study, the city of Wuhan in China was selected as the experimental area. SAR datasets from COSMO-SkyMed (2011-2015), TerraSAR-X (2015-2019), and Sentinel-1 (2019-2021) were fused to map long-term surface deformation over the past decade. An independent InSAR time series analysis from 2011 to 2020, based on 230 COSMO-SkyMed scenes, was used as a reference for comparison. The correlation coefficient between the fusion algorithm's results and the reference data is 0.87 in the time overlapping region and 0.97 in the time-interval dataset. The overall correlation coefficient of 0.78 demonstrates that the proposed algorithm achieves a similar trend as the reference deformation curve. Based on the long time series settlement results obtained through fusion, a detailed analysis of the causes of settlement was conducted for several subsidence zones. The subsidence in the Houhu area is primarily attributed to the consolidation and compression of soft soil. Soil mechanics were employed to estimate the expected completion time of subsidence and calculate the degree of consolidation for each year. The COSMO-SkyMed PSInSAR results indicate that the area has entered the late stage of consolidation and compression, gradually stabilizing over time. Furthermore, the subsidence curve observed in the area around Xinrong reveals that the construction of an underground section of subway Line 21 has caused significant settlement in that particular region. The high temporal granularity of the PSInSAR time series also enables precise detection of a rebound phase following a major flooding event in 2016. The experimental results demonstrate the accuracy of the proposed fusion method in providing robust time series for analyzing long-term land subsidence mechanisms. Additionally, these findings unveil previously unknown characteristics of land subsidence in Wuhan, thus clarifying the relationship with urban causative factors.

1. INTRODUCTION

Urban subsidence is a gradual process characterized by the gradual sinking of the ground surface over time, leading to substantial damage. It is influenced by a combination of human and natural factors (Herrera et al., 2020). Wuhan, the largest city in central China, serves as an illustrative example where the severe impacts of urban subsidence have been observed. The subsidence in Wuhan can be attributed to various human factors, including groundwater extraction and underground construction projects like the subway system. Additionally, natural factors such as soil consolidation and collapses due to karst geology have also played a role in the subsidence occurring in the city (Jiang et al., 2021).

Interferometric Synthetic Aperture Radar (InSAR) technology offers significant advantages, including high spatial and temporal resolution, as well as wide coverage of SAR images (Li et al., 2022). It has emerged as a reliable tool for monitoring urban surface deformation and has replaced traditional measurement methods like leveling and Global Positioning System (GPS).

Numerous studies have been conducted to detect deformation using InSAR technology in Wuhan. (Costantini et al., 2016) and (Zhou et al., 2017) employed image datasets spanning one year to monitor short-term subsidence and analyze the spatio-temporal characteristics and causes of deformation. (Hu et al., 2022) utilized the SBAS method to analyze the consolidation of soft soil and karst collapse hazards in Wuhan, using TerraSAR-X (TSX) imagery collected between 2013 and 2017, along with S1 imagery from 2015 to 2017. (Han et al., 2020) applied the PS-InSAR method to process Envisat (2008-2010), ALOS-1 (2007-2010), and Sentinel-1 (S1) (2015-2019) images. They investigated the effects of urban construction, changes in the Yangtze River, and groundwater levels on the subsidence patterns and trends throughout the city.

However, these studies typically rely on single sensors and have relatively short research periods, usually ranging from 1 to 5 years. The analysis conducted by (Jiang et al., 2021) using COSMO-SkyMed (CSK) data from 2012 to 2019 represents the longest continuous time series study on land subsidence in Wuhan. However, this study still focuses on a single sensor and does not establish connections between multiple sensors. In the case of slow-developing geological hazards like land subsidence, it is recommended to conduct observations for over ten years to accurately determine long-term trends in urban infrastructure and the associated level of risk. Therefore, the fusion of InSAR datasets from multiple satellite platforms in a time-series manner holds significant strategic importance.

2. STUDY AREA AND DATASETS

2.1 STUDY AREA

Wuhan (29°58'N-31°22'N, 113°41'E—115°5'E) is situated in the eastern part of the Jianghan Plain, in the middle reaches of the Yangtze River (refer to Figure 1). The city's geographical layout is defined by the confluence of the Yangtze River and its major tributary, the Han River, creating three distinct regions: Hankou, Wuchang, and Hanyang (refer to Figure 1). With a network of rivers and lakes, approximately 25% of Wuhan's total area is comprised of water bodies. Wuhan experiences a subtropical monsoon climate, characterized by high humidity and abundant precipitation, ranging from 1150 to 1450 millimeters annually. The majority of rainfall occurs during the months of June to August, accounting for approximately 40% of the total annual precipitation (Jiang et al., 2023).

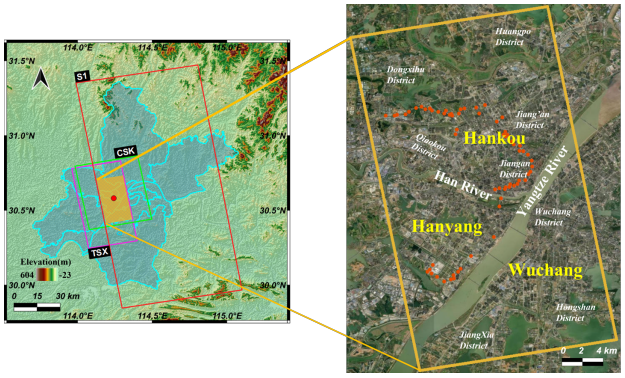

Figure 1. Research area map of Wuhan. Orange dots represent the levelling benchmark.

Wuhan encompasses a carbonate rock area spanning 1100 square kilometers, which constitutes approximately 13% of the urban region. This area comprises six carbonate rock belts. Hankou predominantly consists of flood deposits, resulting in an alluvial plain with widespread distribution of loamy soil. More than 15 instances of subsidence have been recorded due to geological factors. As outlined in the Wuhan Geological Hazard Prevention and Control Plan for 2016-2020, the city includes one high-risk geological hazard area, six central risk zones, four low-risk zones, and one non-risk zone (Bai et al., 2016).

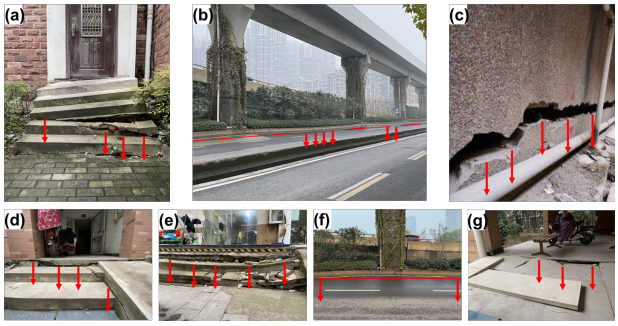

Figure 2. Field investigation of Wuhan subsidence.

2.2 DATASETS

To investigate the long-term subsidence trend in Wuhan, three SAR data stacks were collected, comprising 230 images from the Italian Space Agency (ASI) CSK, 51 images from the German Aerospace Center (DLR) TSX, and 30 images from the German Aerospace Center (DLR) S1. The coverage area of each sensor can be seen in Figure 1. It should be noted that although additional images, such as S1, were available in the archives, they were intentionally excluded from our experimental design. This decision was made to simulate various scenarios of data availability, overlap, and gaps. Consequently, the CSK dataset was manually divided to conclude at the end of 2015, encompassing only the first 89 scenes. As depicted in Figure 3, there is a temporal overlap between the CSK and TSX datasets from January to December 2015. Additionally, there is a time gap between the TSX and S1 datasets spanning from February to June 2019.

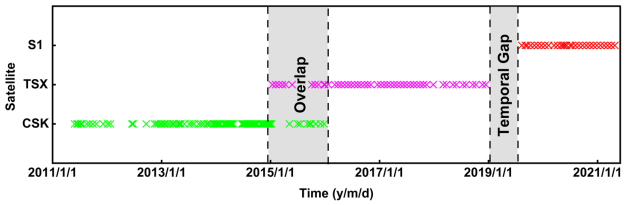

Figure 3. The three satellite datasets selected for the experiment.

A 30-meter resolution SRTM digital elevation model (DEM) was employed for PS-InSAR processing to eliminate the effects of terrain phase. To validate the InSAR results obtained, a set of 60 precise leveling benchmark observations was chosen from the Wuhan Surveying and Mapping Institute. These observations spanned the years 2013-2014, 2015-2016, and 2019-2020 and possessed an accuracy of approximately 2 mm. To establish the periodicity of the deformation time series, optical images from Google Earth were utilized for matching purposes.

3. METHODOLOGY

3.1 InSAR processing

The datasets are processed using the standard PS-InSAR technique (Ferretti et al., 2000, Ferretti et al., 2001) and SARPROZ software. The signal stability of radar targets is assessed using quality parameters, and PS points are obtained by combining these parameters. A strong first-order network is employed to estimate height and velocity parameters. This network consists of a sub-selection of PS candidates (PSC) with an amplitude stability index (ASI) greater than 0.8. Atmospheric phase components are detected and removed during this estimation process. For each point, the line-of-sight (LOS) deformation rate and time series are estimated using a nonlinear trend model. The output datasets from the high-resolution sensors (TSX and CSK) are resampled to match the resolution of the low-resolution sensor (S1), resulting in a final resolution of 30 meters.

3.2 Data fusion approach

3.2.1 Case 1: time series overlaps Based on prior knowledge, it has been observed that the subsidence characteristics in the Wuhan area generally follow an S-shaped curve (Jiang et al., 2023). During the initial stage of surface subsidence, the cumulative deformation increases rapidly, and the subsidence rate accelerates over time. This indicates a positive subsidence acceleration during this stage. In the subsequent stage, the subsidence rate gradually reaches its maximum value, while the

subsidence acceleration gradually decreases and eventually becomes zero. As the subsidence progresses into the attenuation stage, the cumulative deformation continues to increase, but at a slower rate. Therefore, during this stage, the subsidence rate gradually approaches zero. Consequently, the subsidence acceleration transitions from negative to zero. To comprehensively model the entire subsidence process, the Power Exponential Knothe Model can be utilized. This model is capable of capturing the various stages of subsidence, including the initial acceleration, maximum subsidence rate, and attenuation phases (Lei et al., 2018).

$$W(t) = W_{\max}\left(1 - e^{-ct}\right)^k \tag{1}$$

Where $W(t)$ represents the cumulative variable at time t, W_{max} represents the predicted maximum deformation variable, and c and k are the shape parameters to be estimated. Nonlinear least squares combined with a genetic algorithm (GA) is used to rapidly estimate the global optimal solution for the three parameters (W_{max}, c, k) of the PEKM model.

3.2.2 Accurate determination of fusion time After fitting curves to two time series datasets for fusion, it is important to accurately determine the fusion time point "t" to ensure the accuracy of the fusion process (Chen et al., 2021). Many data fusion methods often overlook this crucial issue and choose the fusion time randomly or simply based on the start/end time of the two datasets. However, such approaches may impact the accuracy of the fusion result. To address this, we propose a more accurate approach for determining the fusion time "t" by considering the minimum value of the gradients (velocity) of the two curves in the overlapping region. By analyzing the gradient difference between the two curves, we can identify the point in time where the deformed curve trends are almost the same. This time point is selected as the fusion point.

$$t = \arg\min\left\{\left|d_1'\left(t_i\right) - d_2'\left(t_i\right)\right|\right\}, t_i \in t_1 \cup t_2 \tag{2}$$

Where d_1 and d_2 are the fitted curves of the sedimentation time series for the two input datasets.

3.2.3 Case 2: temporal gaps In cases where there are time intervals in the time series, we consider an alternative fusion strategy. We utilize an LSTM (Long Short-Term Memory) network to predict the sedimentation trend during the gap period and merge it with the subsequent sedimentation curve. LSTM is a special type of recurrent neural network (RNN) (Alex, 2020) that effectively addresses the issues of vanishing and exploding gradients that may occur when using traditional RNNs, thanks to its unique gating mechanism. We will skip explaining the basic principles of LSTM and directly introduce its usage process.

The specific workflow for combining PS-InSAR monitoring results and LSTM for time series prediction includes:

1. Data processing. Time series deformation data is first derived from PS-InSAR. It is transformed into an equal time interval data set using interpolation. Normalization of this dataset is carried out.
2. Training the network. The first 90% of the dataset is used as the training set and the last 10% is kept as the test set. The Adam optimization function is used as the optimizer to update the network weights and initialize the model parameters. The mean square error is chosen as the model loss function, means of which are used to determine the reasonableness of the parameters.
3. Prediction output. The trained network is used to predict the surface deformation and output the prediction results.

4. RESULTS AND DISCUSSION

4.1 InSAR accuracy assessment

To ensure comparability among the three datasets, we carefully selected the same reference point during the processing stage. In order to validate the accuracy of the InSAR results, we compared the computed subsidence values from the CSK, TSX, and S1 datasets with 60 corresponding leveling measurements taken at different time points in Figure 4. The experiment revealed that the InSAR measurements from all three datasets exhibited a strong correlation with the leveling data, with correlation coefficients exceeding 80%. Furthermore, the maximum root mean square error was found to be only 2.85mm, indicating a high level of overall consistency.

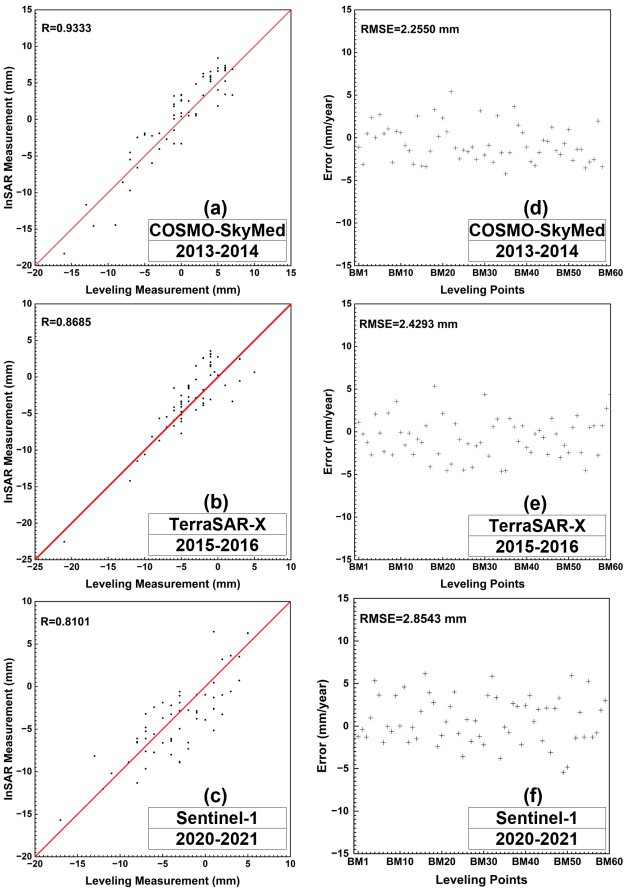

Figure 4. Comparison between leveling and InSAR.

4.2 Fusion results

4.2.1 Overlapping period In the case of temporal overlap, we extracted the deformation time series and fitted curves representing the reference point from the merged CSK and TSX datasets, as depicted in the Figure 5. The table within the figure presents the three parameters estimated using nonlinear least squares combined with a genetic algorithm. The calculated R^2 values for the two fitted curves are 0.9851 and 0.9812, respectively, demonstrating the accuracy of the proposed method in this study. Through calculations, the time point t (2015/12/02) was determined as the fusion time point.

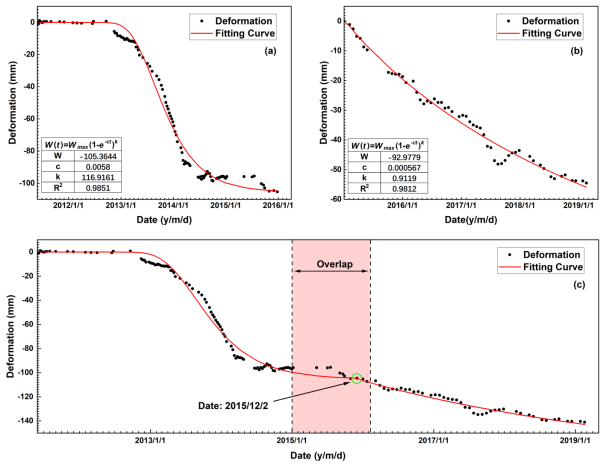

Figure 5. Overlapping period fitting and fusion results. (a) Fitting curve of COSMO-SkyMed, (b) fitting curve of TerraSAR-X, and (c) fusion result.

4.2.2 Temporal gaps In each LSTM layer, the number of neurons is set to 50. The Mean Squared Error (MSE) is utilized as the loss function. The gradient of the MSE loss increases with the rise in the loss but gradually diminishes as the loss approaches 0. This property of the MSE loss ensures rapid convergence and precise training outcomes. The efficient Adam optimizer is selected for its high computational efficiency, and the number of epochs is set to 70. The Adam algorithm keeps track of the First Moment Estimation of the gradients, which is the average of all past gradients and the current gradient. This ensures that the gradients in each update are not drastically different from the previous updates, resulting in smooth and stable gradient transitions that can adapt to unstable target functions. Furthermore, to validate the accuracy of the model, 70% of the data is used for training, and the remaining 30% is used for testing.

Next, the LSTM is utilized to predict the missing data from February to June 2019 (at the end of the TSX time series, as shown in Figure 3). These predicted results are combined with the subsequent S1 data using the minimum gradient method to obtain the complete longest time series deformation from 2011 to 2021 for the test PS point curve, as illustrated in Figure 6.

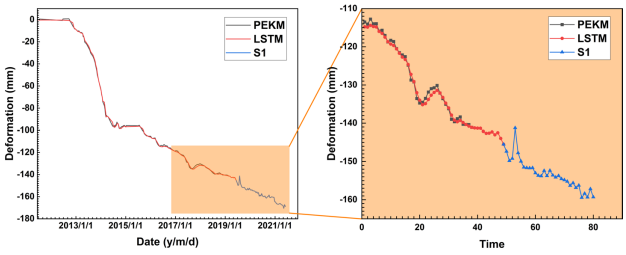

Figure 6. Temporal gap prediction and fusion result.

We observed a high level of consistency between the algorithm's predictions and the reference PS-InSAR deformation curve, with no anomalous values detected. This indicates the reliability of the algorithm. The fusion time point selected using the minimum gradient difference method also resulted in a very smooth fusion curve. Figure 7 presents a comparison between the fusion results from 2011 to 2021 and the CSK reference time series from 2011 to 2020. The fused deformation curve closely aligns with the reference curve, providing evidence of the fusion algorithm's accuracy.

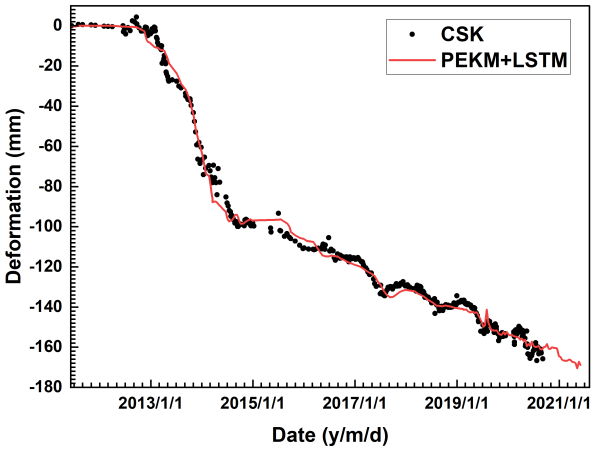

Figure 7. Conparison of the proposed algorithm with CSK result.

4.3 Time-lapse subsidence over Wuhan

Figure 8 illustrates the urban-scale subsidence map derived from the fused subsidence time series, presenting the cumulative annual subsidence from 2012 to 2021. This map provides a clear visualization of the evolving subsidence trend in the Wuhan region.

In the HanKou area, subsidence started in 2013 and gradually intensified over time. The maximum subsidence occurred between 2017 and 2018 and subsequently reached a stable state. This subsidence can be primarily attributed to the consolidation of soft soil in the area. Additionally, it has been observed that the large-scale construction projects and subway line development in the region have contributed to the subsidence, as reported in our previous study (Jiang et al., 2021). However, the longer subsidence time series obtained in this research indicates that the subsidence in the HanKou area stabilized by 2018. On the other hand, in the WuChang and HongShan areas, subsidence started later, around 2016-2017, and continued until 2021.

4.4 Analysis of Factors Contributing to Subsidence

4.4.1 Natural Factors: The Wuhan region is known for its abundance of soft soil, primarily composed of lacustrine deposits that formed during the late Pleistocene period. In various locations, particularly the primary terraces (Figure 2b), the soft soil layer exceeds a thickness of 10 meters. The regular fluctuations in the water level of the surrounding lakes contribute to sediment migration. As a result of slow fluctuations and gentle water flow, the transported sediment gradually settles at the bottom of the lakes, forming a layer of silt-like soft soil.

On the other hand, the rapid urban development in Wuhan has led to the expansion of the built-up area. Construction activities make use of receding lakes, ponds, and reclaimed land. In certain areas, artificial lake filling is employed to increase available land. While lake filling can facilitate urban expansion, the consolidation process of the silty soft soil foundation requires a significant amount of time, particularly evident in the Houhu area. Geological surveys indicate the presence of a silt-like soft soil layer with a thickness exceeding 5 meters beneath the Houhu area.

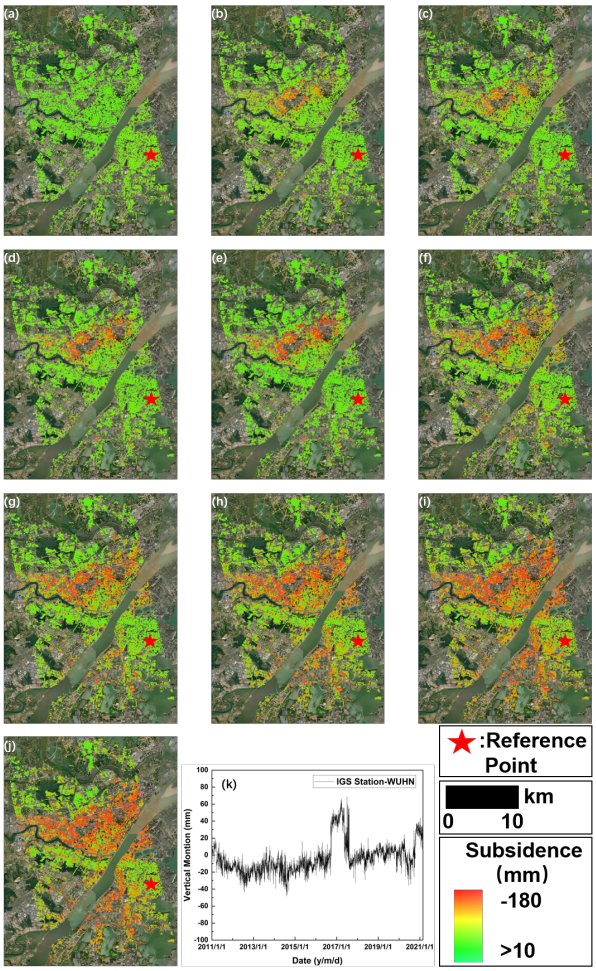

Figure 8. Time-lapse of subsidence in Wuhan based on the fused results, from 2012 (a) to 2021 (j). (k) Vertical motion of reference point i.e. IGS station(wuhn).

In the Houhu area, prior to the end of September 2013, the initial deformation rate resulting from soft soil consolidation and compression was relatively slow. This period was characterized by stability, with minimal deformation rates and limited magnitude, resulting in minimal damage to buildings. It was not expected for large-scale collapses to occur. From the end of 2013 to early 2015, the area entered an intermediate stage of compression and consolidation of the soft soil, during which the vertical reinforcement rate accelerated. At four monitoring points (PS points), the minimum deformation rate reached 50 mm/year, while the maximum reached 115 mm/year. Significant deformation occurred within a short period. During this stage, building foundation damage was severe, and instances of ground and wall cracking were predominantly observed (Figure 4c, d). After February 2015, the compression of the reinforced soft soil was essentially completed, and the deformation rate gradually stabilized, entering the late stage of soft soil reinforcement.

4.4.2 Human factors: From 2012 to 2019, Wuhan underwent extensive subway line construction, including lines 3, 6, 7, 8, 11, and 21, which covered the main urban area. However, the excavation of subway tunnels can lead to ground subsidence above the tracks, as observed in InSAR literature and Wuhan. One notable area affected by this subsidence is the

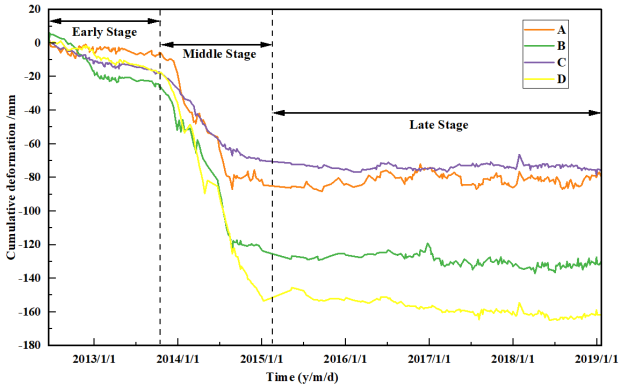

Figure 9. Cumulative deformation map of Houhu.

Xinrong area, where subway lines 1 and 21 intersect. The resettlement center is situated at this intersection.

Subway Line 21's construction began in December 2014 and was completed and opened in January 2018. During this period, four representative PS (Permanent Scatterer) points were selected along the line. The cumulative deformation curve, shown in Figure 10, illustrates the subsidence in the Xinrong area. The subsidence began in October 2014, slightly before the commencement of subway construction. This initial subsidence was due to the need to keep the groundwater level below the estimated construction depth in the first half of the year. By preventing water flowback through pumping, the pore water pressure decreased, resulting in increased effective stress and subsequent surface deformation. Significant surface deformation at this location started to occur in December 2014.

The COSMO-SkyMed InSAR time series provided high temporal sampling, enabling the detection of deformation trend reversals. From April 2016 to July 2016, the deformation trend was limited in time, stabilizing and then recording several months of uplift with magnitudes of 10-15 millimeters. Notably, this period coincided with a sharp increase in rainfall compared to other years, as indicated by monthly average precipitation data. In July 2016, Wuhan experienced a major flood, the most severe in nearly two decades. The flood event halted underground construction, and the areas along the Yangtze River, including the vicinity of the Xinrong area, were primarily affected by the rapid rise in water levels. The significant rainfall and floodwater replenished the groundwater, leading to increased pore water pressure, which slowed down the surface subsidence rate and even caused temporary localized uplift. Construction resumed after the flood, and the subsidence curve displayed a clear linear deformation pattern (Figure 10). As subway construction was completed by early 2018, widespread subsidence gradually ceased. Recent studies based on Sentinel-1 data suggest that land uplift during significant river water level rise can sometimes be subtle. However, in this case, the COSMO-SkyMed data facilitated the observation of these phenomena, which were particularly relevant. The deformation trend reversal was evident and easily detectable.

5. CONCLUSION

This paper presents a method for effectively combining InSAR deformation time series datasets from different SAR missions and/or time periods to overcome the practical challenges encountered when analyzing multi-sensor data for assessing long-term land subsidence. The proposed method integrates the

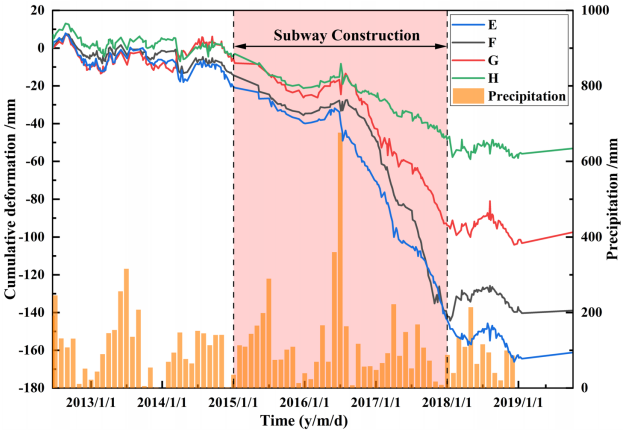

Figure 10. Cumulative deformation map of Xinrong.

PEKM (Power Exponential Knothe Model) algorithm with the LSTM (Long Short-Term Memory) algorithm to handle datasets that have overlapping periods and temporal gaps in the multi-sensor time series. The city of Wuhan is chosen as the experimental area, and datasets from CSK, TSX, and S1 are collected and fused to generate the longest possible time series of subsidence curves in the Wuhan area. The reliability of the method is demonstrated by comparing the results with a reference deformation time series and subsidence trends reported in existing studies. Additionally, an analysis is conducted to identify the natural and anthropogenic factors contributing to subsidence in the Wuhan area. The findings indicate that subsidence in the Houbu area aligns with the consolidation of soft soil model and is influenced by local groundwater management practices. Similarly, the deformation at Xinrong Station is affected by groundwater extraction, construction timing, and the specific impact of the 2016 flood event. These results emphasize the significance of integrating multi-sensor data, providing a more dependable foundation for investigating the mechanisms of subsidence in the Wuhan area.

REFERENCES

Alex, S., 2020. Fundamentals of Recurrent Neural Network (RNN) and Long Short-Term Memory (LSTM) network. *Physica D: Nonlinear Phenomena*, 404, 132306. https://linkinghub.elsevier.com/retrieve/pii/S0167278919305974.

Bai, L., Jiang, L., Wang, H., Sun, Q., 2016. Spatiotemporal Characterization of Land Subsidence and Uplift (2009–2010) over Wuhan in Central China Revealed by TerraSAR-X InSAR Analysis. *Remote Sensing*, 8(4), 350. https://www.mdpi.com/2072-4292/8/4/350. Number: 4 Publisher: Multidisciplinary Digital Publishing Institute.

Costantini, M., Bai, J., Malvarosa, F., Minati, F., Vecchioli, F., Wang, R., Hu, Q., Xiao, J., Li, J., 2016. Ground deformations and building stability monitoring by COSMO-SkyMed PSP SAR interferometry: Results and validation with field measurements and surveys. *2016 IEEE International Geoscience and Remote Sensing Symposium (IGARSS)*, 6847–6850. ISSN: 2153-7003.

Ferretti, A., Prati, C., Rocca, F., 2000. Nonlinear subsidence rate estimation using permanent scatterers in differential SAR interferometry. *IEEE Transactions on Geoscience and Remote Sensing*, 38(5), 2202–2212. http://ieeexplore.ieee.org/document/868878/.

Ferretti, A., Prati, C., Rocca, F., 2001. Permanent Scatterers in SAR Interferometry. *IEEE TRANSACTIONS ON GEOSCIENCE AND REMOTE SENSING*, 39(1).

Han, Y., Zou, J., Lu, Z., Qu, F., Kang, Y., Li, J., 2020. Ground Deformation of Wuhan, China, Revealed by Multi-Temporal InSAR Analysis. *Remote Sensing*, 12(22), 3788. https://www.mdpi.com/2072-4292/12/22/3788. Number: 22 Publisher: Multidisciplinary Digital Publishing Institute.

Herrera, G., Ezquerro, P., Tomás, R., Bejar, M., Vinielles, J. L., Rossi, M., Mateos, R., Carreon, D., Lambert, J., Teatini, P., Cabral-Cano, E., Erkens, G., Galloway, D., Hung, W.-C., Kakar, N., Sneed, M., Tosi, L., Wan, H., Ye, S., 2020. Mapping the global threat of land subsidence. *Science*, 371, 34–36.

Hu, J., Motagh, M., Guo, J., Haghighi, M. H., Li, T., Qin, F., Wu, W., 2022. Inferring subsidence characteristics in Wuhan (China) through multitemporal InSAR and hydrogeological analysis. *Engineering Geology*, 297, 106530. https://linkinghub.elsevier.com/retrieve/pii/S0013795222000151.

Jiang, H., Balz, T., Cigna, F., Tapete, D., 2021. Land Subsidence in Wuhan Revealed Using a Non-Linear PSInSAR Approach with Long Time Series of COSMO-SkyMed SAR Data. *Remote Sensing*, 13(7), 1256. https://www.mdpi.com/2072-4292/13/7/1256.

Jiang, H., Balz, T., Cigna, F., Tapete, D., Li, J., Han, Y., 2023. Multi-sensor InSAR time series fusion for long-term land subsidence monitoring. *Geo-spatial Information Science*, 1–17. https://www.tandfonline.com/doi/full/10.1080/10095020.2023.2178337.

Lei, C., Xuesheng, Z., Yixian, T., Hong, Z., Chen, L., Zhao, X., Tang, Y., Zhang, H., 2018. Parameters fitting and evaluation of exponent Knothe model combined with InSAR technique. *Rock and Soil Mechanics*, 39(Supp.2), 423–431. titleTranslation: titleTranslation: titleTranslation: titleTranslation: titleTranslation: titleTranslation: titleTranslation: titleTranslation: titleTranslation: titleTranslation: titleTranslation: titleTranslation:.

Li, J., Li, Y., Jiang, H., Zhao, Q., 2022. Hierarchical Transmission Tower Detection from High-Resolution SAR Image. *Remote Sensing*, 14, 625.

Zhou, L., Guo, J., Hu, J., Li, J., Xu, Y., Pan, Y., Shi, M., 2017. Wuhan Surface Subsidence Analysis in 2015–2016 Based on Sentinel-1A Data by SBAS-InSAR. *Remote Sensing*, 9(10), 982. http://www.mdpi.com/2072-4292/9/10/982.